scientific reports

Check for updates

OPEN

# Thermal expansion coefficient of few-layer $MoS_2$ studied by temperature-dependent Raman spectroscopy

Zhongtao Lin[1,2], Wuguo Liu[1,3], Shibing Tian[1], Ke Zhu[1], Yuan Huang[1]✉ & Yang Yang[1]✉

**The thermal expansion coefficient is an important thermal parameter that influences the performance of nanodevices based on two-dimensional materials. To obtain the thermal expansion coefficient of few-layer $MoS_2$, suspended $MoS_2$ and supported $MoS_2$ were systematically investigated using Raman spectroscopy in the temperature range from 77 to 557 K. The temperature-dependent evolution of the Raman frequency shift for suspended $MoS_2$ exhibited prominent differences from that for supported $MoS_2$, obviously demonstrating the effect due to the thermal expansion coefficient mismatch between $MoS_2$ and the substrate. The intrinsic thermal expansion coefficients of $MoS_2$ with different numbers of layers were calculated. Interestingly, negative thermal expansion coefficients were obtained below 175 K, which was attributed to the bending vibrations in the $MoS_2$ layer during cooling. Our results demonstrate that Raman spectroscopy is a feasible tool for investigating the thermal properties of few-layer $MoS_2$ and will provide useful information for its further application in photoelectronic devices.**

Two-dimensional (2D) transition metal dichalcogenides (TMDs), especially monolayer 2D TMDs, have attracted enormous attention in the past decade because of not only their striking physical properties[1,2] but also their potential applications in electronic, photonic and thermoelectric devices[3–6]. However, obtaining large-area single crystalline monolayer 2D TMDs is still challenging, hindering their applications in devices. Compared with monolayer 2D TMDs, few-layer 2D TMDs are much easier to achieve by physical or chemical methods. In recent years, few-layer 2D TMDs have received increasing attention due to their interesting physical properties and applications in electronic and optoelectronic devices[7–11]. Neri and coauthors reported the strain induced semiconductor–metal transition in few-layer $MoS_2$[7]. High-speed vertical photodiodes based on few-layer $MoS_2$ have been fabricated using asymmetric metal contacts, exhibiting an external quantum efficiency of up to 7%[9]. A simple few-layer $MoS_2$-based photodetector employing vertical Schottky junctions of Au-$MoS_2$-indium tin oxide (ITO) was proposed by Gong et al.[11]. It has been demonstrated that the physical properties of $MoS_2$ can be significantly affected by the interactions between $MoS_2$ and the substrate, which causes strain, doping and defects[12–16]. One of the prominent substrate effects is the strain created on the $MoS_2$ layer due to the difference in binding energies and the lattice mismatch between the substrate and $MoS_2$. Additionally, the electronic structure of $MoS_2$ can be modulated by external strain, and the PL emission of $MoS_2$ will change as a result[16–18].

The self-heating effect occurs while a device is working under a current flow or light irradiation, so the thermal properties of few-layer $MoS_2$ are important criteria that affect the performance of related electronic and optical devices. For example, the thermoelectric energy conversion ability of $MoS_2$ is related to the low thermal conductivity[19], whereas high performance of electronic devices requires high thermal conductivity[20]. Alongside the thermal conductivity and thermal transport properties, the thermal expansion coefficient is another important thermal property of $MoS_2$. The thermal expansion coefficient (TEC) mismatch between the substrate and $MoS_2$ introduces additional internal strain to the $MoS_2$ layer. Consequently, the optical and electronic performances of $MoS_2$ devices supposedly change due to the thermal strain. Therefore, clear insight into the TEC of

[1]Beijing National Laboratory for Condensed Matter Physics, Institute of Physics, Chinese Academy of Sciences, P O Box 603, Beijing 100190, People's Republic of China. [2]Faculty of Materials and Manufacturing, Beijing University of Technology, Beijing 100124, People's Republic of China. [3]Department of Materials Science and Engineering, and State Key Laboratory of Heavy Oil Processing, College of Science, China University of Petroleum Beijing, No. 18 Fuxue Rd., Beijing 102249, People's Republic of China. ✉email: yhuang01@iphy.ac.cn; yang.yang@iphy.ac.cn

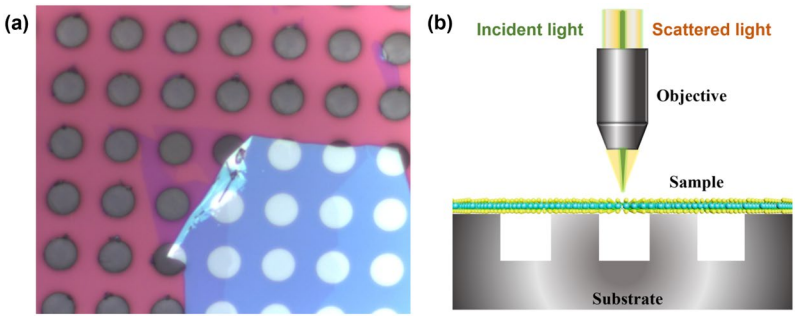


**Figure 1.** (**a**) Optical image of 2-layer $MoS_2$ on a prepatterned $SiO_2$/Si substrate with a 5 μm hole array. (**b**) Schematic illustration of Raman measurement for $MoS_2$ suspended on microholes.

$MoS_2$, especially the TEC mismatch between $MoS_2$ and the substrate, is a key for studying the thermal stability and intrinsic optical properties of few-layer $MoS_2$-based devices.

Raman spectroscopy has been demonstrated to be a versatile tool for investigating 2D TMDs[21–23]. In the past decade, the temperature effects on the Raman modes of 2D TMDs have been widely investigated[24–29]. However, the temperature behaviors of the Raman peaks of TMDs are still controversial. Some researchers reported that the peak positions varied linearly with increasing temperature[24–27]. Late et al. reported that both monolayer and few-layer $MoSe_2$ and $WSe_2$ exhibit a linear temperature dependence[25]. A linear temperature dependence of Raman modes was also observed in monolayer $Mo_{1-x}W_xS_2$[27]. In recent years, some studies have demonstrated that the temperature dependence of the Raman peak positions for TMDs can be fitted by a nonlinear function. Su and coauthors employed temperature-dependent Raman spectroscopy to study the substrate bonding effects on $MoS_2$ and $WS_2$ and expressed the temperature dependence of Raman modes using a third-order polynomial function[28–30]. Although the reported temperature dependences of Raman modes for 2D TMDs differ, the TEC mismatch between TMDs and substrates is widely accepted to play an important role in the temperature evolution of Raman modes. To eliminate the substrate effects, suspended TMDs have been used to study the intrinsic properties of TMDs in recent years[31–36]. Two-ten times improvement of the mobility and on/off ratio was observed in suspended monolayer $MoS_2$[31]. The elastic coefficients, including the 2D elastic modulus and Young's modulus, were obtained for suspended multilayer $WSe_2$[32]. Moreover, the intrinsic thermal conductivity has been investigated for monolayer and few-layer $MoS_2$[33,34]. However, to our knowledge, the TEC mismatch effect in few-layer $MoS_2$ has not been systematically studied, and the intrinsic TEC of few-layer $MoS_2$ has not yet been obtained.

In this work, suspended $MoS_2$ and supported few-layer (2–6 layer) $MoS_2$ was comprehensively investigated using Raman spectroscopy in the temperature range from 77 to 557 K. The temperature dependence of suspended $MoS_2$ exhibited different trends from that of supported few-layer $MoS_2$, which could be attributed to the TEC mismatch between $MoS_2$ and the substrate. Moreover, the temperature dependence of the Raman modes varied with the number of layers. Removing the substrate effect by adopting suspended $MoS_2$ as a freestanding $MoS_2$, the intrinsic TECs of few-layer $MoS_2$ was obtained. Prominent differences between our results and previous reports were observed and discussed in detail.

## Results and discussion

The suspended and supported samples were fabricated by transferring $MoS_2$ with 2–6 layers onto microholes, which were prepared using a modified mechanical exfoliation method[37] (see "Methods"). Figure 1a presents the optical microscopy image of suspended 2-layer $MoS_2$ as an example.

Raman spectra were collected using a confocal micro-Raman spectrometer (Horiba Evolution) under backscattering geometry, as exhibited in Fig. 1b. Figure 2 presents the room-temperature Raman spectra of suspended and supported few-layer $MoS_2$, which exhibit the typical spectral features of $MoS_2$ previously reported[22,23]. Two high frequency peaks appear at approximately 380 $cm^{-1}$ and 405 $cm^{-1}$, originating from the lattice vibration of bulk $MoS_2$. Due to the crystalline symmetry changes between bulk, monolayer and few-layer $MoS_2$, the symmetric representations of these two Raman modes are different. For convenience, these two modes are identified as the $E_{2g}$ and $A_{1g}$ modes, respectively, following the assignments for bulk $MoS_2$[23]. The bulk-vibrational Raman modes shift to higher positions with increasing number of layers. In recent years, ultralow frequency (ULF) Raman spectroscopy has attracted the interest of more researchers because it has been demonstrated to be a feasible tool for studying the interlayer vibrational modes of TMDs[38–40]. The ULF Raman peaks originate from the in-plane (shear) and out-of-plane (breathing) vibrations of $MoS_2$, which have been used to identify the number of $MoS_2$ layers[39,40]. The sharp peak is denoted as a shear mode (S1), while the broad peak is assigned as a breathing mode (B1), as shown in Fig. 2. Notably, the signal-to-noise ratio (SNR) of the Raman peaks, especially the ULF Raman peaks, of suspended $MoS_2$ is much better than that of supported $MoS_2$, and more detailed spectral information can be clearly seen. Both the S1 and B1 modes are clearly observed on suspended $MoS_2$, whereas only the S1 mode is detected on supported $MoS_2$. The $MoS_2$ layer is pinned on the substrate through van der Waals forces. The dielectric environment created from by the substrate may have effect on the local electromagnetic field due to the multiple reflection inside the monolayer[16]. The enhanced Raman signal of the suspended $MoS_2$ can be attributed to the isolation from the substrate effect[35]. Moreover, the $E_{2g}$ mode for the supported 2L $MoS_2$ is asymmetric, as shown in Fig. 2b. As Mignuzzi et al. reported, defects could induce not only an asymmetric line shape but also

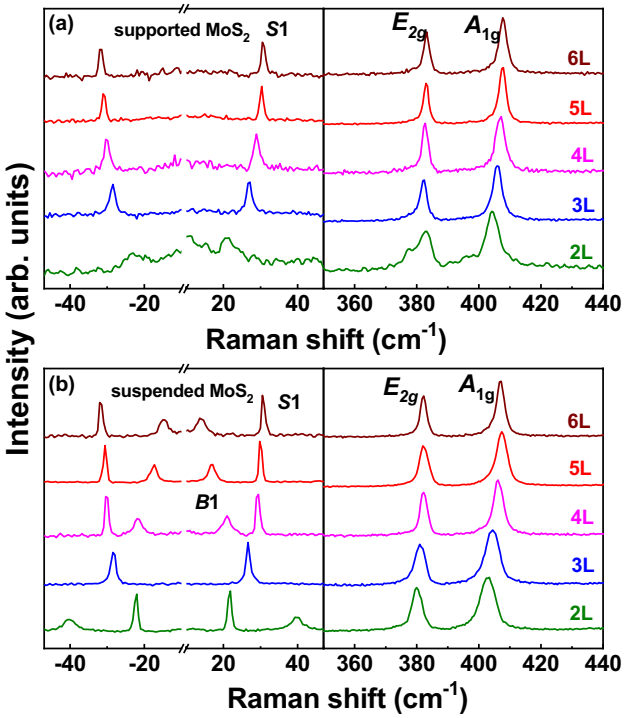


**Figure 2.** Raman spectra of (**a**) supported and (**b**) suspended $MoS_2$ with different numbers of layers collected at room temperature.

Raman peaks arising from zone-edge phonon modes[41]. In our work, no additional peak was observed in the spectrum for supported 2L $MoS_2$, suggesting that the strain is the dominant effect rather than defects. The $E_{2g}$ mode of monolayer $MoS_2$ has been demonstrated to split into two singlets as the external strain is increased[42,43]. As presented in Fig. S1b, the $E_{2g}$ mode can be well fitted using two peaks, which can be attributed to the strain introduced by the substrate-$MoS_2$ interaction. We assume that the substrate-induced strain is the same for all the supported $MoS_2$ flakes. Therefore, the strain effect on the supported 2L $MoS_2$ is the most obvious because 2L $MoS_2$ is thinner than the other samples.

To deeply investigate the substrate effect, supported $MoS_2$ and suspended few-layer $MoS_2$ were studied in the temperature range of 77 K–557 K, and the results are displayed in Fig. 3. Prominent redshift and broadening of Raman peaks are noted for both suspended and supported $MoS_2$ with increasing temperature, as exhibited in Fig. 3. These phenomena can be attributed to the thermal expansion of the crystal lattice of $MoS_2$[26,27].

To obtain deeper insight into the difference between suspended and supported $MoS_2$, the Raman spectra were deconvoluted using a Lorentz/Gaussian mixed function. The peak positions of the $E_{2g}$ and $A_{1g}$ modes are plotted as a function of temperature in one figure for comparison. Figure 4 exhibits the fitting results for supported and suspended $MoS_2$, in which several remarkable phenomena should be addressed, as discussed below.

First, the temperature-dependent evolutions of the supported $MoS_2$ samples are similar, varying approximately linearly with increasing temperature at first sight. This suggests that the substrate effect is exerted on the $MoS_2$ flakes as a whole, although the substrate is only in direct contact with the bottom layer of a $MoS_2$ flake. The mechanically exfoliated $MoS_2$ layer is transferred and pinned on the substrate by the van der Waals force. As the temperature changes, the biaxial tensile or compressive stress induced by the TEC mismatch increases and becomes a prominent factor that modulates the frequency shift of Raman peaks. In addition to TEC mismatch, charge transfer between the film and the substrate or through interfacial states can impact the temperature evolution of Raman peak. As Su et al. discussed that accelerated redshift of $A_{1g}$ mode with increasing temperature is associated with the enhanced charge injection from the substrate into the film and decomposition of adsorbed contaminants[30].

Second, the temperature-dependent evolutions of suspended $MoS_2$ are very different from those of supported $MoS_2$, exhibiting nonlinear behavior with increasing temperature. Moreover, the temperature dependence trends for the different suspended $MoS_2$ samples differ. As discussed previously, the TEC mismatch gives rise to a Raman shift with increasing temperature. However, suspended $MoS_2$, at least the part on the hole, is free of the substrate effect, suggesting that its Raman shift only originates from lattice expansion. Compared with the temperature dependence of supported $MoS_2$, suspended few-layer $MoS_2$ exhibits the intrinsic thermal properties of $MoS_2$ as expected.

Third, the peak positions of supported $MoS_2$ are higher than those of suspended $MoS_2$ at each temperature, suggesting that the TEC mismatch induced compression of the crystalline lattice in supported $MoS_2$. That the larger attached area of supported $MoS_2$ compared with suspended $MoS_2$ would introduce more strain into the

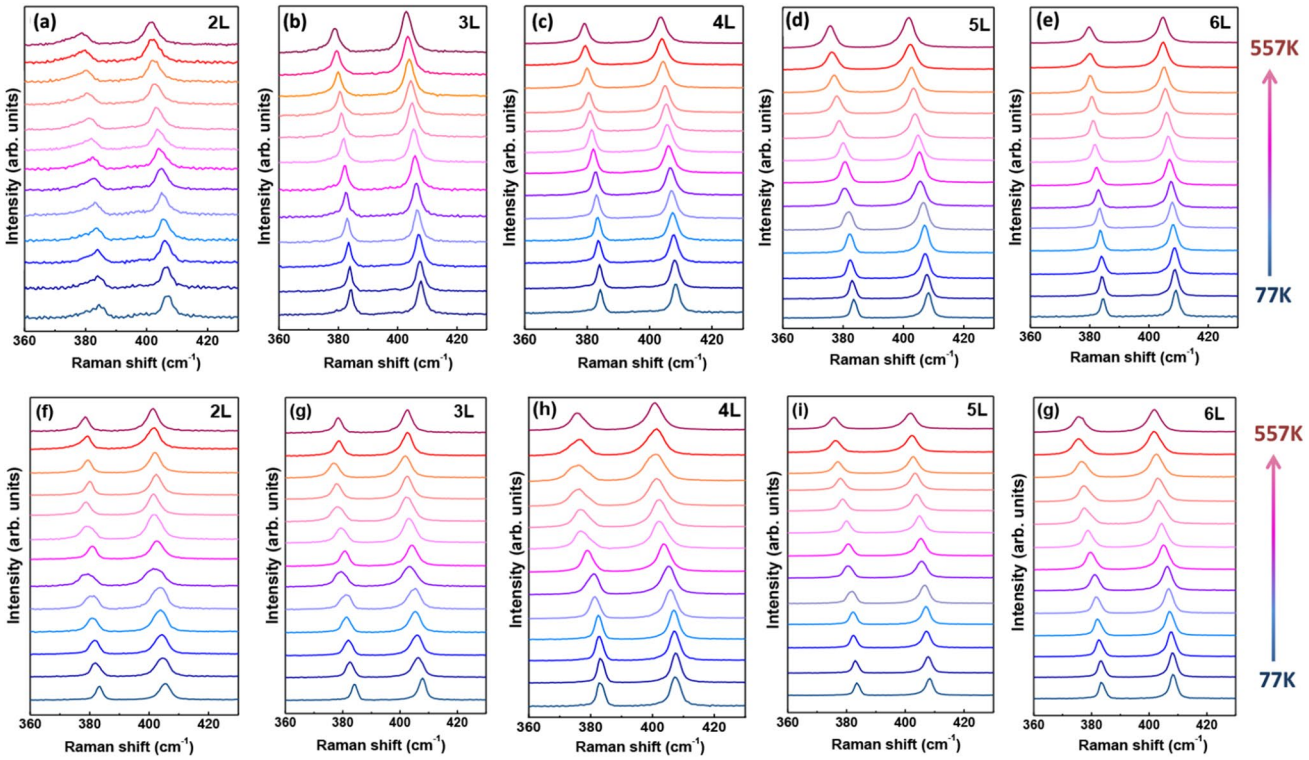


**Figure 3.** Raman spectra of (**a**–**e**) supported and (**f**–**g**) suspended few-layer $MoS_2$ for different temperatures.

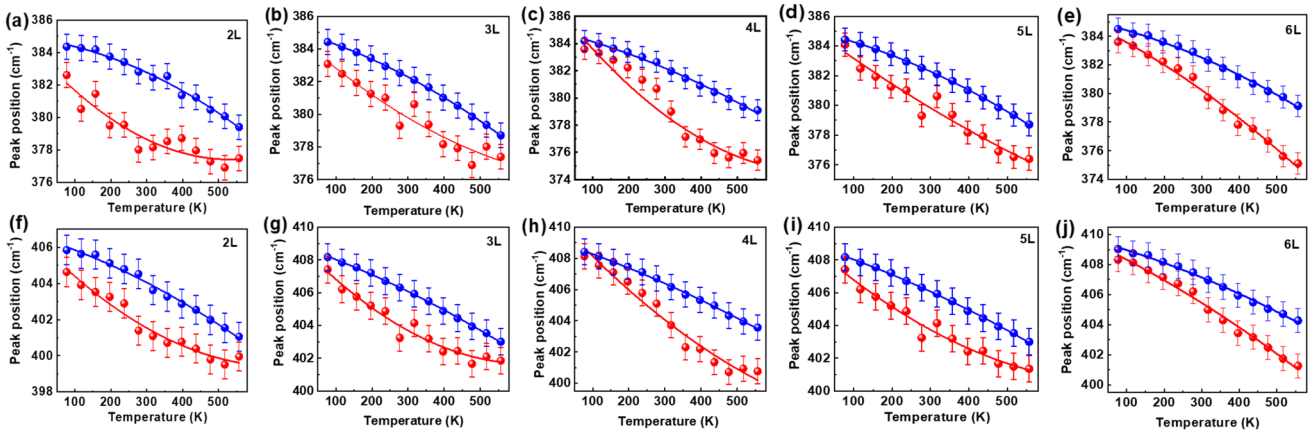


**Figure 4.** Temperature dependence of peak positions of the (**a**–**e**) $E_{2g}$ and (**f**–**j**) $A_{1g}$ modes for the suspended and supported $MoS_2$ with different numbers of layers. The blue spheres and red spheres represent the experimental results of supported and suspended $MoS_2$, respectively. The blue lines and red lines are the fitting results obtained using a second-order polynomial function of temperature.

$MoS_2$ layer is easy to explicate. As demonstrated previously, the strain in the $MoS_2$ layer is due to the TEC mismatch between the $SiO_2$ substrate and $MoS_2$.

The results shown in Fig. 4 demonstrate that the TEC of $MoS_2$ is strongly correlated with the number of layers, which can only be obviously exhibited after isolating it the from the substrate effect.

Then, the peak positions of $MoS_2$ were fitted as a function of temperature to obtain the regularities of the temperature dependence of the peak positions. First, a linear function was employed to fit temperature evolution Raman peaks for the supported and suspended $MoS_2$ samples (see Fig. S2). The temperature evolution of Raman peaks for the supported $MoS_2$ shows a nearly linear behavior as a function of temperature. But there is a small deviation between the experimental results and fitting curve, as exhibited in Fig. S2. On the other hand, the temperature evolution for the suspended $MoS_2$ cannot be well fitted using a linear function, in which large discrepancies between the linearly fitted curves and experimental results are observed. According to previous literatures, the anharmonic effect caused by the phonon–phonon coupling leads to the nonlinear temperature-dependent behavior of the Raman peaks[28].

| | | $E_{2g}$ mode | | | $A_{1g}$ mode | | |
|---|---|---|---|---|---|---|---|
| | | $\omega_0$ | $\chi_1$ | $\chi_2$ | $\omega_0$ | $\chi_1$ | $\chi_2$ |
| 2L | Sus | 383.835 | − 0.024 | $2.249\times10^{-5}$ | 406.271 | − 0.020 | $1.490\times10^{-5}$ |
| | Sup | 384.812 | − 0.003 | $-1.153\times10^{-5}$ | 406.550 | − 0.006 | $-6.557\times10^{-6}$ |
| 3L | Sus | 385.948 | − 0.029 | $2.622\times10^{-5}$ | 409.181 | − 0.026 | $2.334\times10^{-5}$ |
| | Sup | 384.995 | − 0.006 | $-8.833\times10^{-6}$ | 408.843 | − 0.008 | $-5.139\times10^{-6}$ |
| 4L | Sus | 386.710 | − 0.033 | $2280\times10^{-5}$ | 410.519 | − 0.025 | $1.168\times10^{-5}$ |
| | Sup | 384.884 | − 0.007 | $-7.127\times10^{-6}$ | 409.096 | − 0.008 | $-4.157\times10^{-6}$ |
| 5L | Sus | 384.990 | − 0.019 | $5.616\times10^{-6}$ | 408.667 | − 0.020 | $1.236\times10^{-5}$ |
| | Sup | 384.214 | − 0.008 | $-1384\times10^{-5}$ | 409.105 | − 0.011 | $-5.266\times10^{-6}$ |
| 6L | Sus | 384.935 | − 0.013 | $-9.845\times10^{-6}$ | 409.585 | − 0.012 | $-6.340\times10^{-6}$ |
| | Sup | 385.099 | − 0.006 | $-8.738\times10^{-6}$ | 409.719 | − 0.007 | $-5.627\times10^{-6}$ |

**Table 1.** Temperature coefficients of the suspended and supported few-layer $MoS_2$ samples with polynomial fitting to the second order.

Therefore, the polynomial function was adopted to fit the experimental results for the supported and suspended $MoS_2$ samples instead of the linear function. All the temperature dependence trends of the $E_{2g}$ and $A_{1g}$ modes were fitted using a second-order polynomial function of temperature $T$,

$$\omega(T) = \omega_0 + \chi_1 T + \chi_2 T^2 \tag{1}$$

where $\omega_0$ is the frequency at 0 K and $\chi_1$ and $\chi_2$ are the first- and second-order temperature coefficients, respectively. The fitting results for supported and suspended $MoS_2$ with the same thickness are plotted in Fig. 4 for comparison, and the fitting parameters are listed in Table 1. As shown in Fig. 4, the polynomial curves better fit the experimental results for the supported and suspended $MoS_2$, compared with the linear curves. Remarkably, for the supported $MoS_2$, the residual sum of square (RSS) for the polynomial fitting is much smaller than that for the linear fitting (see Table S1 in the Supplementary Information). This implies that the polynomial function is a better and more reasonable choice for fitting the temperature-evolution of the Raman shifts for the supported $MoS_2$, although it exhibits an approximate linear trace.

As exhibited in Table 1, the fitting parameters for suspended $MoS_2$ are very different from those for supported $MoS_2$. The fitting parameter $\chi_1$ for suspended $MoS_2$ is one order of magnitude larger than that for supported $MoS_2$. Moreover, the fitting parameters exhibit a layer number dependence. As exhibited in Table 1, for the 2L–5L $MoS_2$ samples, the $\chi_2$ of suspended $MoS_2$ is positive, whereas the $\chi_2$ of supported $MoS_2$ is negative. Interestingly, $\chi_2$ is negative for both suspended and supported 6L $MoS_2$. This occurs because of the different temperature evolutions of 6L $MoS_2$ and thinner $MoS_2$. One can see in Fig. 4e and j that the peak positions for the 6L suspended $MoS_2$ linearly shift to low frequency, similar as the peak evolution for the supported $MoS_2$. Therefore, the fitting parameters for the curves are all negative. In contrast, the shift rates of the peak positions for the 2L–5L suspended $MoS_2$ vary in different temperature ranges. As exhibited in Fig. 4a–d, the peak positions shift faster in the low temperature range (< 350 K) than in the high temperature range (> 350 K). Therefore, the parameter $\chi_2$ is positive to better fit the experimental results. The thermal stability of $MoS_2$ strongly depends on the competition between the energy barriers introduced by the $MoS_2$–substrate interface and by the $MoS_2$–$MoS_2$ interlayer interface[44]. The few-layer $MoS_2$ flake as a whole changes with increasing temperature, the influence of the intrinsic thermal expansion of $MoS_2$ on the frequency shift increases as the number of layers increases. As a result, the temperature evolutions of the Raman peaks of the suspended and supported 6L $MoS_2$ samples become similar. These results suggest that the thermal behavior of few-layer $MoS_2$ become similar as that of bulk $MoS_2$ with increasing thickness.

The results in Table 1 indicate that the discrepancy in the frequency shifts between the suspended and supported $MoS_2$ originates from the TEC mismatch between the substrate and $MoS_2$. Taking advantage of the results shown in Figs. 3, 4 and 5, the TEC of few-layer $MoS_2$ can be obtained, and the details for the calculation of the TEC of few-layer $MoS_2$ will be discussed in the following section.

As has been reported, the temperature-dependent Raman frequency shift ($\Delta\omega_{MoS2}(T)$) of freestanding $MoS_2$ can be commonly attributed to the thermal expansion of the lattice ($\Delta\omega^E(T)$) and the anharmonic effect ($\Delta\omega^A(T)$), which changes the phonon self-energy[45]. $\Delta\omega_{MoS2}(T)$ can be expressed as

$$\Delta\omega_{MoS2}(T) = \Delta\omega^E(T) + \Delta\omega^A(T) \tag{2}$$

$\Delta\omega_{MoS2}(T)$ can be obtained using the peak position at $T$ ($\omega_{MoS2}(T)$) subtracted by the peak position at $T_0 = 300$ K ($\omega_{MoS2}(T_0)$).

For the thermal behavior of the supported $MoS_2$, both common thermal effects and strains induced by the TEC mismatch between the substrate and $MoS_2$ must be considered. As a result, the frequency shifts of supported $MoS_2$ can be written as

$$\Delta\omega^S_{MoS2}(T) = \Delta\omega^E(T) + \Delta\omega^A(T) + \Delta\omega^S(T) \tag{3}$$

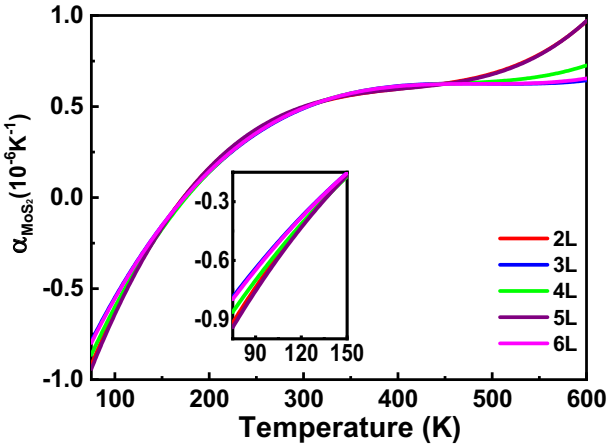


**Figure 5.** Calculated TECs of $MoS_2$ with different numbers of layers. The inset figure shows a magnified view of the TECs in the temperature range of 75–150 K.

The $E_{2g}$ mode arises from the in-plane relative vibration between the Mo and S atoms, which is more sensitive to the temperature-induced lattice expansion/shrinkage of 2D $MoS_2$. On the other hand, the frequency shift of $A_{1g}$ mode not only closely depends on lattice variations, but also is related with the charge transfer from the substrate to $MoS_2$[46]. The electron doping effect can induce the frequency shifts of $A_{1g}$ mode due to the strong electron–phonon interaction[47]. Consult to previous literature, the $E_{2g}$ mode is not sensitive to the electron doping effect[47,48]. So it is assumed that the electron doping effect induced Raman shift of $E_{2g}$ mode did not change with temperature, or the changes can be neglected. For simplicity, the doping effect induced Raman shift of $E_{2g}$ mode is defined as a constant that is independent of temperature in this work. Thus, in the calculation of the Raman frequency differences ($\Delta\omega_{MoS2}(T)$) between the given temperatures and $T = 300$ K, the doping effect induced Raman shift is subtracted as a constant. So that there are still three terms in Eq. (3) when the doping effect induced Raman shift is not taken into consideration. Therefore, the $\Delta\omega_{MoS2}(T)$ of $E_{2g}$ mode was calculated and employed in the following equations.

The TEC mismatch-induced frequency shift can be obtained by subtracting the intrinsic frequency shift from the frequency shift of supported $MoS_2$,

$$\Delta\omega^S(T) = \Delta\omega^S_{MoS2}(T) - \Delta\omega_{MoS2}(T) \tag{4}$$

To apply Eq. (4), the frequency shift of freestanding $MoS_2$ should be provided. However, real freestanding $MoS_2$ does not exist. Therefore, Raman frequency shifts from theoretical calculations or suspended TMDs have normally been employed as those of freestanding samples[31,35]. In this work, we assume that the strain induced by the substrate effect can be neglected in the center of the suspended $MoS_2$ layers, as the laser spot (1 μm) in the measurement is much smaller than the size of the hole (5 μm) below the suspended $MoS_2$. Therefore, the Raman shifts of suspended $MoS_2$ is adapt as the intrinsic frequency of freestanding $MoS_2$ in this work.

Based on above discussion, the TEC mismatch-induced frequency shift $\Delta\omega^S(T)$ for the supported $MoS_2$ can be obtained by

$$\Delta\omega^S(T) = \Delta\omega_{sup}(T) - \Delta\omega_{sus}(T) \tag{5}$$

where $\Delta\omega_{sup}(T)$ and $\Delta\omega_{sus}(T)$ are the Raman shifts of supported and suspended $MoS_2$, respectively.

In addition, the contribution to the Raman frequency shift from the substrate-induced strain ($\Delta\omega^S(T)$) can be expressed as

$$\Delta\omega^S(T) = \beta\int_{T_0}^{T}[\alpha_{SiO_2}(T) - \alpha_{MoS_2}(T)] \tag{6}$$

where $\beta$ is the biaxial strain coefficient of the Raman mode and $\alpha_{SiO_2}(T)$ and $\alpha_{MoS_2}(T)$ are the temperature-dependent TECs of $SiO_2$ and $MoS_2$, respectively. As has been reported, $\beta$ depends on the number of $MoS_2$ layers[49].

As the values of $\alpha_{SiO_2}$ and $\beta$are already known from previous literatures, the temperature dependence of $\alpha_{MoS_2}$ can be derived from Eqs. (5) and (6). The calculated $\alpha_{MoS_2}(T)$ can be expressed using a quadratic function, and then, the $\alpha_{MoS_2}(T)$ values for $MoS_2$ with different numbers of layers are plotted in Fig. 5.

As presented in Fig. 5, the curves of the calculated TECs of $MoS_2$ with different numbers of layers follow similar trends. Notably, the order of magnitude of the TECs is at the same level as those in previous reports[22,28], implying the validity of the calculation methods employed in this work. For example, the TEC at room temperature observed in this work is approximately $0.5\times10^{-6}$ $K^{-1}$. Su et al. claimed that the in-plane TEC of $MoS_2$ is $2.48\times10^{-6}$ $K^{-1}$ at room temperature[28], whereas Late et al. reported a TEC of $8.2\times10^{-6}$ $K^{-1}$[22]. The discrepancy in the TECs between our results and previous publications can be attributed to the diversity in $\beta$ employed in the calculation and whether the substrate effect is considered. Remarkably, the TECs of few-layer $MoS_2$ are very close

in the temperature range of 150–450 K. These results clearly suggest the feasibility of using Raman spectroscopy in the investigation of the TEC of $MoS_2$, at least in the temperature range of 150–450 K.

In addition, the diversity in the TECs between the $MoS_2$ with different numbers of layers is also obvious. As presented in the inset figure of Fig. 5, the TECs of few-layer $MoS_2$ exhibit remarkable differences in the temperature ranges of 0–150 K and 450–600 K. Strikingly, the TEC becomes negative below 175 K. This is different from most previous reports[25,28,50,51], in which the TEC is positive in the entire temperature range. In 2015, Wang et al. obtained a negative TEC below 31 K for monolayer $MoS_2$ using first-principles calculation by taking the stiffness and charge transfer effect into consideration[52]. The ZA bending vibrations (acoustic modes) may cause negative thermal expansion in few-layer $MoS_2$[52,53]. The negative value of the Grüneisen parameter for the transverse acoustic mode responds for the negative TEC[54]. The larger the absolute value of the negative Grüneisen parameter is, the larger the negative TEC. The negative TEC below 175 K observed in our work suggests a larger negative Grüneisen parameter.

Moreover, the TEC of few-layer $MoS_2$ increases gently in the temperature range over 450 K, as shown in Fig. 5. This evolution of the TEC observed in our work is similar to that in previous studies[50–52]. However, the high-temperature TECs for 4L and 5L $MoS_2$ exhibit a slight difference compared with the other thicknesses. Wang et al. reported that the threshold temperature for etching monolayer $MoS_2$ is lower than 513 K, which is closely related with defects[44]. The abnormal behavior of the TECs for 4L and 5L $MoS_2$ in the high temperature range can be attributed to the lower thermal stability due to the defects initially existed in these $MoS_2$ samples. Identification of the TEC of few-layer $MoS_2$ requires further experimental and theoretical studies. In the future, the temperature-dependent Raman study carried with controllable electronic doping concentration is called to deeply investigate the doping and dielectric environment effects on the frequency shifts of Raman modes, especially the $A_{1g}$ mode.

## Conclusion

In this work, a comprehensive Raman study was carried out on supported and suspended $MoS_2$ with different numbers of layers in the temperature range from 77 to 557 K. Strikingly, the temperature behaviors of the Raman frequency shift for suspended $MoS_2$ are significantly different from those for supported $MoS_2$. The intrinsic TECs of 2–6-layer $MoS_2$ were calculated after eliminating the substrate effect. Strikingly, the TEC becomes negative below 175 K, which can be associated with the bending vibration in the $MoS_2$ layer as the temperature decreases. The TEC curves of $MoS_2$ with different numbers of layers follow similar evolution trends in the temperature range of 150–450 K. Compared with previous reports, the validity of the TEC obtained in this work suggests that Raman spectroscopy is a feasible tool for investigating the TEC of $MoS_2$. Our results provide useful information for understanding the thermal properties of $MoS_2$ and its further application in devices.

## Methods

To fabricate suspended $MoS_2$ samples, a periodic hole array was first fabricated on a $SiO_2$ (300 nm)/Si substrate by UV lithography and reactive ion etching technology, in which the holes were 5 μm in diameter and 2 μm in depth. $MoS_2$ flakes with different thicknesses were prepared from a natural $MoS_2$ single crystal using a modified mechanical exfoliation method onto the prepatterned $SiO_2$/Si substrate previously cleaned by oxygen plasma.

The optical image of the suspended few-layer $MoS_2$ was obtained using an Olympus BX41 microscope equipped on the micro-Raman spectrometer, Horiba Evolution HR. In the Raman spectroscopy measurements, a solid-state laser with a 532 nm wavelength was used as the excitation source. The laser beam was focused using a 100 × long-working distance objective with numeric aperture NA = 0.8, and the spot size was approximately 1 μm. To avoid significant frequency shifts induced by the local heating effect and ensure a sufficient SNR, the laser power was set at ~ 0.9 mW on the surface of the heating stage. The numbers of layers of $MoS_2$ were identified using ULF Raman spectroscopy. The sample was placed inside a cryostat cell (Linkam, THMS 600), and the Raman spectra were measured in the temperature range from 77 to 557 K at an interval of 20 K.

Received: 17 July 2020; Accepted: 4 March 2021
Published online: 29 March 2021

## References

1. Wang, J., Deng, S. & Liu, Z. The rare two-dimensional materials with Dirac cones. *Natl. Sci. Rev.* **2**, 22–39 (2015).
2. Pei, J. J., Yang, J. & Zhang, H. Many-body complexes in 2D semiconductors. *Adv. Mater.* **31**, 1706945 (2019).
3. Huang, X., Zeng, Z. & Zhang, H. Metal dichalcogenide nanosheets: Preparation, properties and applications. *Chem. Soc. Rev.* **42**, 1934–1946 (2013).
4. Wang, Q. H., Kourosh, K. Z. & Andras, K. Electronics and optoelectronics of two-dimensional transition metal dichalcogenides. *Nat. Nanotechnol.* **7**, 699–712 (2012).
5. Subbaiah, Y. P. V., Saji, K. J. & Tiwari, A. Atomically thin $MoS_2$: A versatile nongraphene 2D material. *Adv. Funct. Mater.* **26**, 2046–2069 (2016).
6. Kaito, K., Jiang, P. & Taishi, T. 2D materials for large-area flexible thermoelectric devices. *Adv. Energy Mater.* **10**, 1902842 (2020).
7. Neri, I. & Miquel, L. Electronic transport modulation on suspended few-layer $MoS_2$ under strain. *Phys. Rev. B* **95**, 241408 (2018).
8. Yu, F., Liu, Q. & Gan, X. Ultrasensitive pressure detection of few-layer $MoS_2$. *Adv. Mater.* **29**, 1603266 (2017).
9. Hou, X. *et al.* Operation mode switchable charge-trap memory based on few-layer $MoS_2$. *Semicond. Sci. Technol.* **33**, 034001 (2018).
10. Li, Z., Chen, J., Dhall, R. & Stephen, B. C. Highly efficient, high speed vertical photodiodes based on few-layer $MoS_2$. *2D Mater.* **4**, 015004 (2017).
11. Gong, F., Fang, H. H. & Wang, P. Visible to near-infrared photodetectors based on $MoS_2$ vertical Schottky junctions. *Nanotechnology* **28**, 484002 (2017).
12. Liu, Z. *et al.* Strain and structure heterogeneity in $MoS_2$ atomic layers grown by chemical vapour deposition. *Nat. Commun.* **5**, 5264 (2014).

13. Wang, Y., Gaspera, E. D. & Carey, B. J. Enhanced quantum efficiency from a mosaic of two dimensional $MoS_2$ formed onto aminosilane functionalized substrates. *Nanoscale* **8**, 12258–12266 (2016).
14. Buscema, M., Steele, G. A. & Van, Z. H. S. J. The effect of the substrate on the Raman and photoluminescence emission of single-layer $MoS_2$. *Nano Res.* **7**, 561–571 (2014).
15. Bao, W. Z., Cai, X. H., Kim, D. H., Karthik, S. & Michael, S. Fuhrer, High mobility ambipolar $MoS_2$ field-effect transistors: Substrate and dielectric effects. *Appl. Phys. Lett.* **102**, 042104 (2013).
16. Yu, Y. F. *et al.* Engineering substrate interactions for high luminescence efficiency of transition-metal dichalcogenide monolayers. *Adv. Funct. Mater.* **26**, 4733–4739 (2016).
17. Dai, Z. H., Liu, L. Q. & Zhang, Z. Strain engineering of 2D materials: Issues and opportunities at the interface. *Adv. Mater.* **31**, 1805417 (2019).
18. Sun, Y. H. *et al.* Evolution of local strain in Ag-deposited monolayer $MoS_2$ modulated by interface interactions. *Nanoscale* **11**, 22432 (2019).
19. Michele, B. *et al.* Large and tunable photothermoelectric effect in single-layer $MoS_2$. *Nano Lett.* **13**, 358–363 (2013).
20. Peng, B. *et al.* Thermal conductivity of monolayer $MoS_2$, $MoSe_2$, and $WS_2$: Interplay of mass effect, interatomic bonding and anharmonicity. *RSC Adv.* **6**, 5767 (2016).
21. Zhang, X., Tan, Q. H. & Wu, J. B. Review on the Raman spectroscopy of different types of layered materials. *Nanoscale* **8**, 6435–6450 (2016).
22. Lu, X., Luo, X. & Zhang, J. Lattice vibrations and Raman scattering in two-dimensional layered materials beyond graphene. *Nano Res.* **9**, 3559–3597 (2016).
23. Zhang, X., Qiao, X. F. & Shi, W. Phonon and Raman scattering of two-dimensional transition metal dichalcogenides from monolayer, multilayer to bulk material. *Chem. Soc. Rev.* **44**, 2757–2785 (2015).
24. Najmaei, S., Ajayan, P. M. & Lou, J. Quantitative analysis of the temperature dependency in Raman active vibrational modes of molybdenum disulfide atomic layers. *Nanoscale* **5**, 9758–9763 (2013).
25. Late, D. J., Shirodkar, S. N. & Waghmare, U. V. Thermal expansion, anharmonicity and temperature-dependent raman spectra of single- and few-layer $MoSe_2$ and $WSe_2$. *ChemPhysChem* **15**, 1592–1598 (2014).
26. Huang, X., Gao, Y. & Yang, T. Quantitative analysis of temperature dependence of Raman shift of monolayer $WS_2$. *Sci. Rep.* **6**, 32236 (2016).
27. Chen, Y., Wen, W. & Zhu, Y. Temperature-dependent photoluminescence emission and Raman scattering from $Mo_{1-x}W_xS_2$ monolayers. *Nanotechnology* **27**, 445705 (2016).
28. Su, L., Zhang, Y. & Yu, Y. Dependence of coupling of quasi 2-D $MoS_2$ with substrates on substrate types, probed by temperature dependent Raman scattering. *Nanoscale* **6**, 4920–4927 (2014).
29. Su, L., Yu, Y. & Cao, L. Effects of substrate type and material-substrate bonding on high-temperature behavior of monolayer $WS_2$. *Nano Res.* **8**, 2686–2697 (2015).
30. Su, L., Yu, Y. & Cao, L. In situ monitoring of the thermal-annealing effect in a monolayer of $MoS_2$. *Phys. Rev. Appl.* **7**, 034009 (2017).
31. Jin, T., Kang, J. & Su, K. E. Suspended single-layer $MoS_2$ devices. *J. Appl. Phys.* **114**, 164509 (2013).
32. Zhang, R., Koutsos, V. & Cheung, R. Elastic properties of suspended multilayer $WSe_2$. *Appl. Phys. Lett.* **108**, 042104 (2016).
33. Yan, R., Simpson, J. R. & Bertolazzi, S. Thermal conductivity of monolayer molybdenum disulfide obtained from temperature-dependent raman spectroscopy. *ACS Nano* **8**, 986–993 (2014).
34. Aiyiti, A., Hu, S. & Wang, C. Thermal conductivity of suspended few-layer $MoS_2$. *Nanoscale* **10**, 2727–2734 (2018).
35. Lee, J. U., Kim, K. & Cheong, H. Resonant Raman and photoluminescence spectra of suspended molybdenum disulfide. *2D Mater.* **2**, 044003 (2015).
36. Tamulewicz, M. D., Kutrowska-Girzycka, J. & Gajewski, K. R. Layer number dependence of the work function and optical properties of single and few layers $MoS_2$: Effect of substrate. *Nanotechnology* **30**, 245708 (2019).
37. Huang, Y., Sutter, E., Shi, N. N. & Zheng, J. Reliable exfoliation of large-area high-quality flakes of graphene and other two-dimensional materials. *ACS Nano* **9**, 10612–10620 (2015).
38. Liang, L., Zhang, J. & Sumpter, B. G. Low-frequency shear and layer-breathing modes in Raman scattering of two-dimensional materials. *ACS Nano* **11**, 11777–11802 (2017).
39. Zhang, X., Han, W. P. & Wu, J. B. Raman spectroscopy of shear and layer breathing modes in multilayer $MoS_2$. *Phys. Rev. B* **87**, 115413 (2013).
40. Zhao, Y., Luo, X. & Li, H. Inter layer breathing and shear modes in few-trilayer $MoS_2$ and $WSe_2$. *Nano Lett.* **13**, 1007–1015 (2013).
41. Sandro, M. *et al.* Effect of disorder on Raman scattering of single-layer $MoS_2$. *Phys. Rev. B* **91**, 195411 (2015).
42. Wang, Y. L., Cong, C. X., Qiu, C. Y. & Yu, T. Raman spectroscopy study of lattice vibration and crystallographic orientation of monolayer $MoS_2$ under uniaxial strain. *Small* **9**, 2857–2861 (2013).
43. Matěj, V. *et al.* Novoselov, and Otakar Frank, strain and charge doping fingerprints of the strong interaction between monolayer $MoS_2$ and gold. *J. Phys. Chem. Lett.* **11**, 6112–6118 (2020).
44. Wang, X. *et al.* Substrate modified thermal stability of mono- and few-layer $MoS_2$. *Nanoscale* **10**, 3540 (2018).
45. Yoon, D., Son, Y. W. & Cheong, H. Negative thermal expansion coefficient of graphene measured by raman spectroscopy. *Nano Lett.* **11**, 3227–3231 (2011).
46. Dhakal, K. P. *et al.* Confocal absorption spectral imaging of $MoS_2$: Optical transitions depending on the atomic thickness of intrinsic and chemically doped $MoS_2$. *Nanoscale* **6**, 13028–13035 (2014).
47. Chakraborty, B. *et al.* Symmetry-dependent phonon renormalization in monolayer $MoS_2$ transistor. *Phys. Rev. B* **85**, 161403 (2012).
48. Iqbal, M. W., Shahzad, K., Akbar, R. & Hussain, G. A review on Raman finger prints of doping and strain effect in TMDCs. *Microelectron. Eng.* **219**, 111152 (2020).
49. Mccreary, A. *et al.* Effects of uniaxial and biaxial strain on few-layered terrace structures of $MoS_2$ grown by vapor transport. *ACS Nano* **10**, 3186–3197 (2016).
50. Ding, Y. & Xiao, B. Thermal expansion tensors, Gruneisen parameters and phonon velocities of bulk $MT_2$, (M=W and Mo; T=S and Se) from first principles calculations. *RSC Adv.* **5**, 18391–18400 (2015).
51. Yuan, J., Lv, Z. & Lu, Q. First-principles study of the phonon vibrational spectra and thermal properties of hexagonal $MoS_2$. *Solid State Sci.* **40**, 1–6 (2015).
52. Wang, Z. Y., Zhou, Y. L. & Wang, X. Q. Effects of in-plane stiffness and charge transfer on thermal expansion of monolayer transition metal dichalcogenide. *Chin. Phys. B* **24**, 026501 (2015).
53. Abdullaev, N. A., Suleimanov, R. A., Aldzhanov, M. A. & Alieva, L. N. On the role played by bending vibrations in heat transfer in layered crystals. *Phys. Solid State* **44**, 1859 (2002).
54. Sevik, C. Assessment on lattice thermal properties of two-dimensional honeycomb structures: Graphene, h-BN, h-$MoS_2$, and h-$MoSe_2$. *Phys. Rev. B* **89**, 035422 (2014).


## Acknowledgements

The authors acknowledge the financial support received from the National Key Research and Development Program of China (Grant Nos. 2018YFB0703500, 2019YFA0308000, 2018YFA0704201), the National Natural

Science Foundation of China (Grant Nos. 11704401, 11874405), and the Scientific Equipment Development Project of the Chinese Academy of Sciences (Grant No. YJKYYQ20170027).

## Author contributions

Z.L. and W.L. did the measurements, data analysis. K. Z. did part of the data analysis. S. T. and Y. H. prepared the samples. Y. Y. supervised the study and wrote the main manuscript text. All authors reviewed the manuscript.

## Competing interests

The authors declare no competing interests.

## Additional information

**Supplementary Information** The online version contains supplementary material available at https://doi.org/10.1038/s41598-021-86479-6.

**Correspondence** and requests for materials should be addressed to Y.H. or Y.Y.

**Reprints and permissions information** is available at www.nature.com/reprints.

**Publisher's note** Springer Nature remains neutral with regard to jurisdictional claims in published maps and institutional affiliations.